Journal of Alloys and Compounds 776 (2019) 1048–1055

Contents lists available at ScienceDirect

Journal of Alloys and Compounds

journal homepage: http://www.elsevier.com/locate/jalcom

# Raman scattering study on phonon anisotropic properties of SiC

Xiao Qin [a, b], Xiaomeng Li [a, b], Xiufang Chen [a, b, *], Xianglong Yang [a, b], Fusheng Zhang [a, b], Xiangang Xu [a, b, **], Xiaobo Hu [a, b], Yan Peng [a, b], Peng Yu [b, c]

[a] State Key Laboratory of Crystal Materials, Shandong University, Jinan, 250100, PR China
[b] Collaborative Innovation Center for Global Energy Interconnection (Shandong), Jinan, 250061, PR China
[c] State Grid Shandong Electric Power Research Institute, Jinan, 250001, PR China

ARTICLE INFO

*Article history:*
Received 14 August 2018
Received in revised form
26 September 2018
Accepted 25 October 2018
Available online 26 October 2018

*Keywords:*
SiC
Phonon
Anisotropic
Raman selection rules

ABSTRACT

Phonon anisotropic properties of 4H, 6H and 15R-SiC were investigated by polarization Raman scattering, and Raman selection rules were explored both theoretically and experimentally. As a function of the relative angles between the incident and the scattered light, Raman intensity of $E_1$, $E_2$ and $A_1$ modes were collected from the (0001) plane, the $(1\bar{1}00)$ plane, and the $(11\bar{2}0)$ plane of wurtzite SiC and the 15R-SiC region in the (0001) plane. Results showed that $E_1$, $E_2$ and $A_1$ modes were anisotropic in the $(11\bar{2}0)$ and the $(1\bar{1}00)$ planes of 4H and 6H-SiC, while $E_2$ modes were isotropous in the (0001) plane. Furthermore, $E_1$ mode of 799 $cm^{-1}$ in the (0001) plane appeared and exhibited anisotropic properties due to the stacking faults in SiC. Otherwise, the anisotropic properties of $A_1$ and E modes of 15R-SiC in the (0001) plane were in agreement with that of wurtzite SiC.



## 1. Introduction

Silicon carbide (SiC), one of the third generation wide band gap semiconductor materials with high thermal conductivity and novel electronic properties is commonly used in the fabrication of high-frequency, high-temperature and high-power devices [1–5]. Due to the different stacking patterns, there are more than 200 crystal forms [6], including cubic, hexagonal, and rhombohedral structures. Currently, the preparation and properties of semiconductor materials have become the key factors in determining device performance and development. However, the structural characterization of SiC is still incomplete. SiC single crystal has been extensively studied in material growth, mass analysis, optical properties, electronic structure, etc., but detailed analysis of its anisotropic properties is still lacking, which is of great significance for understanding the SiC structure and promoting the application of the SiC devices. The Raman study on phonon anisotropic properties is utilized to provide more bases for the application of SiC. Since a specific phonon mode can be enhanced or attenuated by selectively exciting the crystal, it may be applied to nonlinear optical devices in the future.

Raman spectroscopy has been widely used as a nondestructive and effective method for characterizing semiconductor materials by revealing the information of the sample quality, the phonon interactions and the dynamics [7]. Anisotropic properties of wurtzite gallium nitride (GaN) [8–10] and zinc oxide (ZnO) [11] have been extensively studied by the polarization Raman spectroscopy. At present, the characterization of SiC by Raman is mainly used to distinguish the crystal form [12–15], evaluate the stress and explore the doped concentration [16–19]. Nevertheless, reports about the applications of polarization Raman to investigate the phonon anisotropic properties in different polar planes [20] of 4H, 6H and 15R-SiC crystals are almost absent.

Hexagonal wurtzite SiC is a tetrahedrally coordinated semiconductor compound belonging to the space group $C_{6v}^4$ ($P6_3mc$), and 15R-SiC polytype belongs to the trigonal system with its space group $C_{3v}^5$. The weak submodules in the first-order Raman scattering of hexagonal wurtzite 4H and 6H-SiC can be subdivided into axial ($A_1$) and planar ($E_1$ and $E_2$) modes according to the motion directions of atoms [21–23]. According to theoretical predictions, Raman active modes of 4H, 6H and 15R-SiC including $3A_1+3E_1+4E_2$, $5A_1+5E_1+6E_2$, $9A_1+9E$, respectively [21,24]. However, the position and the number of Raman peaks changed on account of the

* Corresponding author. State Key Laboratory of Crystal Materials, Shandong University, Jinan, 250100, PR China.
** Corresponding author. State Key Laboratory of Crystal Materials, Shandong University, Jinan, 250100, PR China.
*E-mail addresses:* xqin412@163.com (X. Qin), cxf@sdu.edu.cn (X. Chen), xxu@sdu.edu.cn (X. Xu).

https://doi.org/10.1016/j.jallcom.2018.10.324
0925-8388/

inability of separating the modes with similar energy of the spectrometer [21–23].

In this paper, Raman spectra were recorded from the (0001) plane, $(1\bar{1}00)$ plane, and $(11\bar{2}0)$ plane of wurtzite SiC and the 15R-SiC region in the (0001) plane. As a function of the relative angles between the incident and the scattered light, phonon anisotropic properties and Raman selection rules of 4H, 6H and 15R-SiC were investigated theoretically and experimentally.

## 2. Experimental

Polarization Raman spectra of SiC were collected by a HR800 Raman spectrometer system from Horiba Jobin Yvon with a 532 nm solid-state laser as the exciting source. Utilizing a 100X objective lens test with a numerical aperture of 0.50, and the focused spot was about 0.75 μm in diameter. The λ/2 waveplate was utilized to control the directions of the incident light, and the polarizer was applied to control the directions of the scattered light entering the analyzer. Raman spectra were acquired in the range of 100–1000 $cm^{-1}$ wave-number by a lens-based spectrometer with a cooled charge-coupled device (CCD) detector.

SiC wafers employed in the measurement were sliced and processed from SiC boules grown by physical vapor transport (PVT) method. As depicted in Fig. 1(b), the $[1\bar{1}00]$, $[11\bar{2}0]$ and [0001] direction was defined as the x-axis, y-axis, and z-axis, respectively. Ulteriorly, the cross section that perpendicular to the x-axis, y-axis and z-axis was recognized as the$(1\bar{1}00)$, $(11\bar{2}0)$ and (0001) plane, respectively. In the experiment, the polarizer was fixed to hold stationary direction of the scattered light while changing the directions of the half-wave plate, as described in Fig. 1(b). More specifically, $e_i$ was known as the unit vector in the direction of the incident light, $e_s$ was considered as the unit vector in the direction of the scattered light. The angle between the unit vector of $e_i$ and $e_s$ was severally presented as θ, β and γ in the (0001) plane, $(11\bar{2}0)$ plane and $(1\bar{1}00)$ plane. Raman spectra of the (0001) plane of 4H, 6H, and 15R-SiC were shown in Fig. 1(c), and the crystal polytype can be distinguished by the peak position of the optical planar mode (FTA) [15,21]. The anisotropy properties of the phonons were discussed by the variety intensity of $E_1$, $E_2$ and $A_1$ modes of 4H, 6H and 15R -SiC in Fig. 1(c). Moreover, different planes of 4H, 6H and 15R-SiC SiC can be distinguished by the High resolution X-ray diffraction, as showed in Table 1 and the supporting information. The deviation of the data in the measurement and the JCPDS cards in Table 1 was due to the miscut angles during the cutting process.

## 3. Results and discussion

### 3.1. Phonon anisotropic properties of wurtzite SiC

Phonon anisotropic properties in the different polar planes of SiC were manifested in the fact that the Raman intensity varies with the relative directions of the incident light and the scattered light (see the supporting information). Fig. 2 presents the Raman spectra of 6H-SiC collected at diverse relative directions of the incident and the

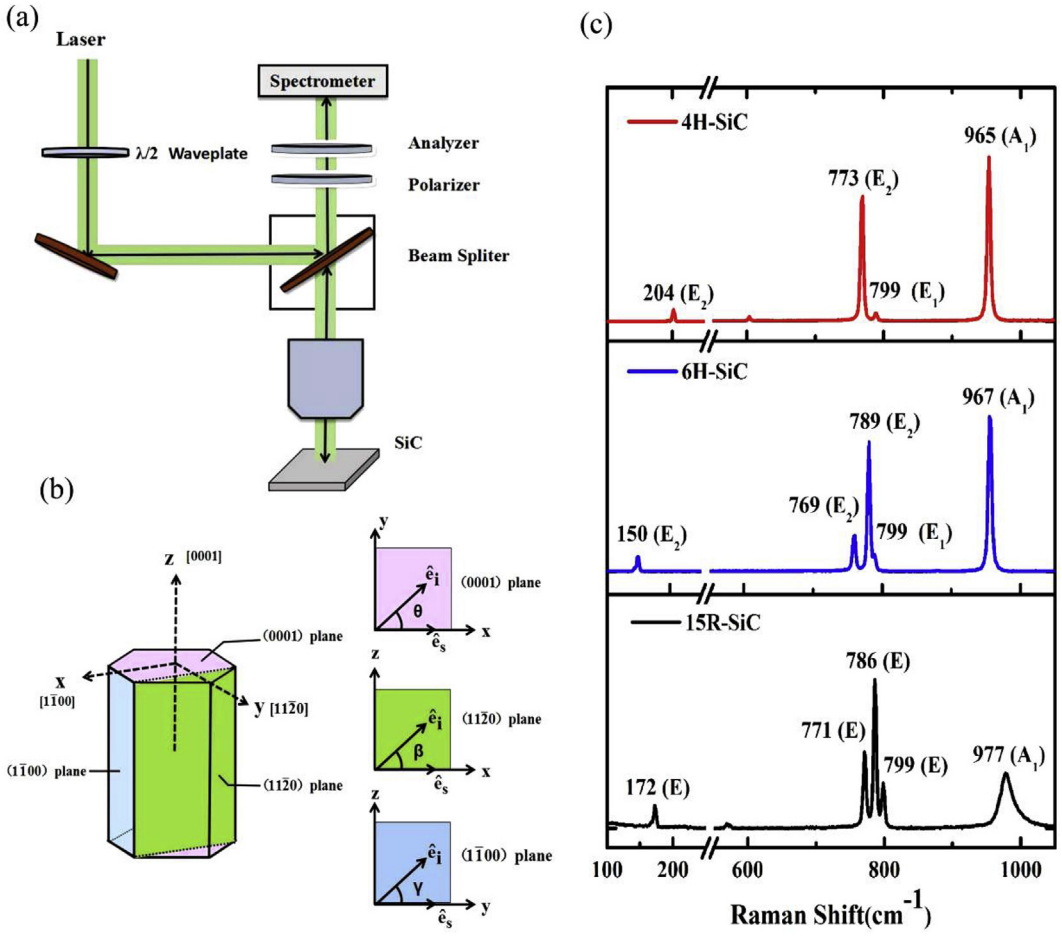


**Fig. 1.** (a) The optical path diagram of the polarization Raman spectrometer. (b) Crystal structure diagrams of hexagonal wurtzite SiC and the experimental configuration for Raman measurements. (c) Raman spectra of the (0001) plane of 4H, 6H, and 15R-SiC.

**Table 1**
High resolution X-ray diffraction results of different SiC plane.

| Polytype | Plane | hkl | $\theta_{cal}$(°) | $\theta_{exp}$(°) | FWHM(sec) |
|---|---|---|---|---|---|
| 4H | (0001)-plane | 004 | 17.850 | 17.681 | 91.43 |
| | $(11\bar{2}0)$- plane | 110 | 30.077 | 27.733 | 43.30 |
| | $(1\bar{1}00)$- plane | 100 | 16.826 | 15.971 | 50.36 |
| 6H | (0001)-plane | 006 | 17.799 | 17.795 | 55.68 |
| | $(11\bar{2}0)$- plane | 110 | 29.994 | 29.987 | 42.04 |
| | $(1\bar{1}00)$- plane | $1\bar{1}0$ | – | 13.713 | 82.71 |
| 15R | (0001)-plane | – | – | 14.692 | 247.23 |

*$\theta_{cal}$: searched in the JCPDS.

scattered light. It was apparent that $E_2$ modes were isotropic in the (0001) plane while the intensity of $A_1$ modes relyed on the relative directions, as showed in Fig. 2(a). However, the intensities of $E_1$, $E_2$ and $A_1$ modes changed regularly with the distinct relative angles in the $(11\bar{2}0)$ and $(1\bar{1}00)$ planes, as indicated in Fig. 2(b) and (c).

Normalized intensities of $E_2$ (789 $cm^{-1}$) mode and $A_1$ (967 $cm^{-1}$) mode in the (0001) plane were collected in the range of $0^\circ \sim 360^\circ$ with the increments of 30° to analyze the phonon anisotropic properties, as showed in Fig. 3(a). Results indicated that the normalized intensity of $A_1$ modes exhibited periodic oscillations and showed a square cosinusoidal dependence on the relative directions between the incident and the scattered light. Moreover, the intensity of $A_1$ modes reached the maximum when the direction of the incident light perpendicular to the direction of the scattered light, and the strength was the smallest when they were parallel. However, the normalized intensity of $E_2$ modes didn't change with the relative directions of the incident and the scattered light, and exhibiting isotropic characteristics.

Fig. 3(b) and (c) indicate the experimental data and fitting curves for the normalized intensity of $E_1$ (799 $cm^{-1}$), $E_2$ (789 $cm^{-1}$) and $A_1$ (967 $cm^{-1}$) modes collected at different relative directions of the incident and the scattered light. It was noticeable that the normalized intensity of $E_1$, $E_2$, and $A_1$ modes exhibited significant periodic variation in the $(11\bar{2}0)$ plane and $(1\bar{1}00)$ plane. The results showed that $E_2$ and $A_1$ modes were consistent in periodic oscillations, while the $E_1$ modes exhibited opposite oscillations completely. Moreover, the normalized intensity of $E_2$ and $A_1$ modes showed a square cosinusoidal dependence on the relative directions of the incident and scattered light while $E_1$ modes exhibited a square sinusoidal dependence.

Identical measurements were performed on 4H-SiC for the purpose of verifying the phonon anisotropic properties of wurtzite SiC, as plotted in Fig. 4. The results revealed that the anisotropic properties of $E_2$, $E_1$, and $A_1$ modes in different polar planes of 4H-SiC were coincident with that of 6H-SiC.

In order to summarize the phonon anisotropy characteristics of wurtzite SiC in different polar planes, theoretical calculations were carried out. Generally described by the derivative of the Raman scattering cross section, the efficiency of Raman scattering of Stokes scattering can be written as [25]:

$$\frac{d\sigma_s}{d\Omega} = \frac{V}{\varepsilon_0 (4\pi)^2} \left(\frac{\omega_S}{c}\right)^4 \left| e_i \bullet \frac{d\alpha}{d\xi} e_s \right|^2 (n_p + 1) \frac{\hbar}{2\omega_V} \quad (1)$$

Where V is the scattering volume, $\omega_S$ is the frequency of the scattered light, $\omega_V$ is the frequency of the molecular vibration mode, $\frac{d\alpha}{d\xi}$ represents the Raman tensor, and $n_p$ is the Bose factor. Consequently, Eq. (1) can be rewritten as

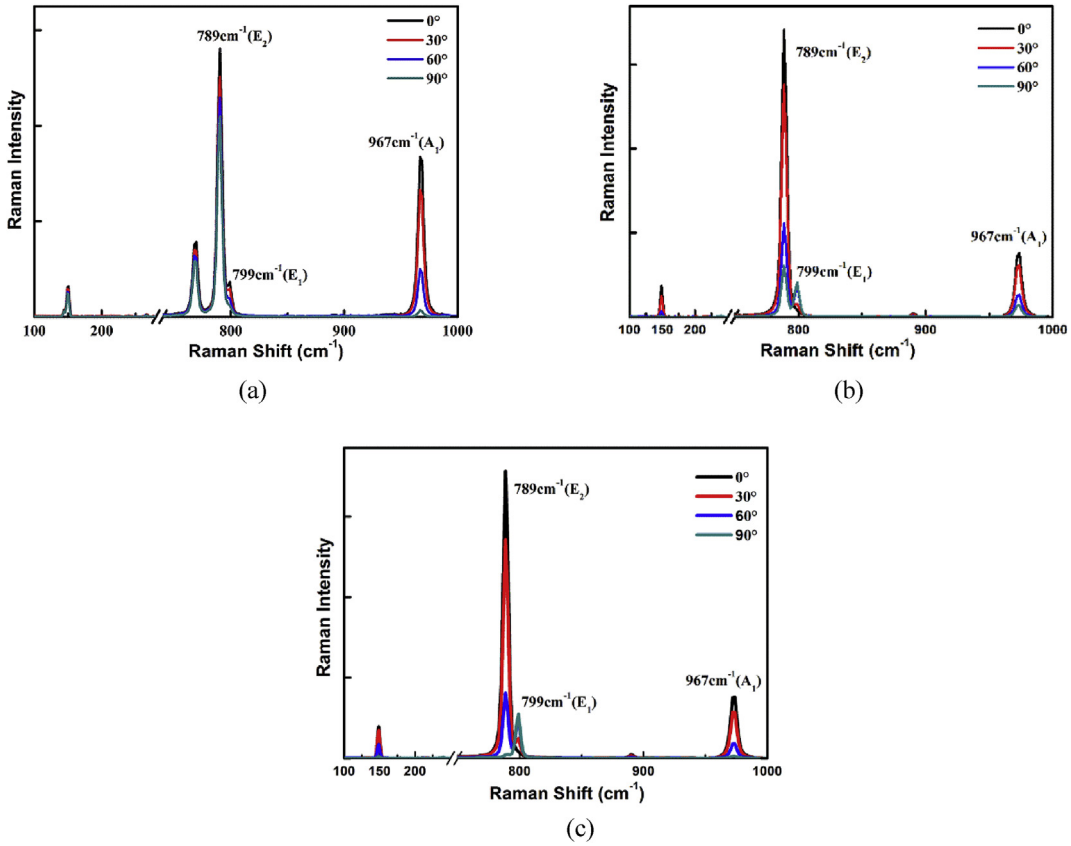


**Fig. 2.** Polarized Raman spectra of 6H-SiC collected at different relative angles between the incident and the scattered light, (a) (0001)-plane, (b) $(11\bar{2}0)$-plane and (c) $(1\bar{1}00)$-plane.

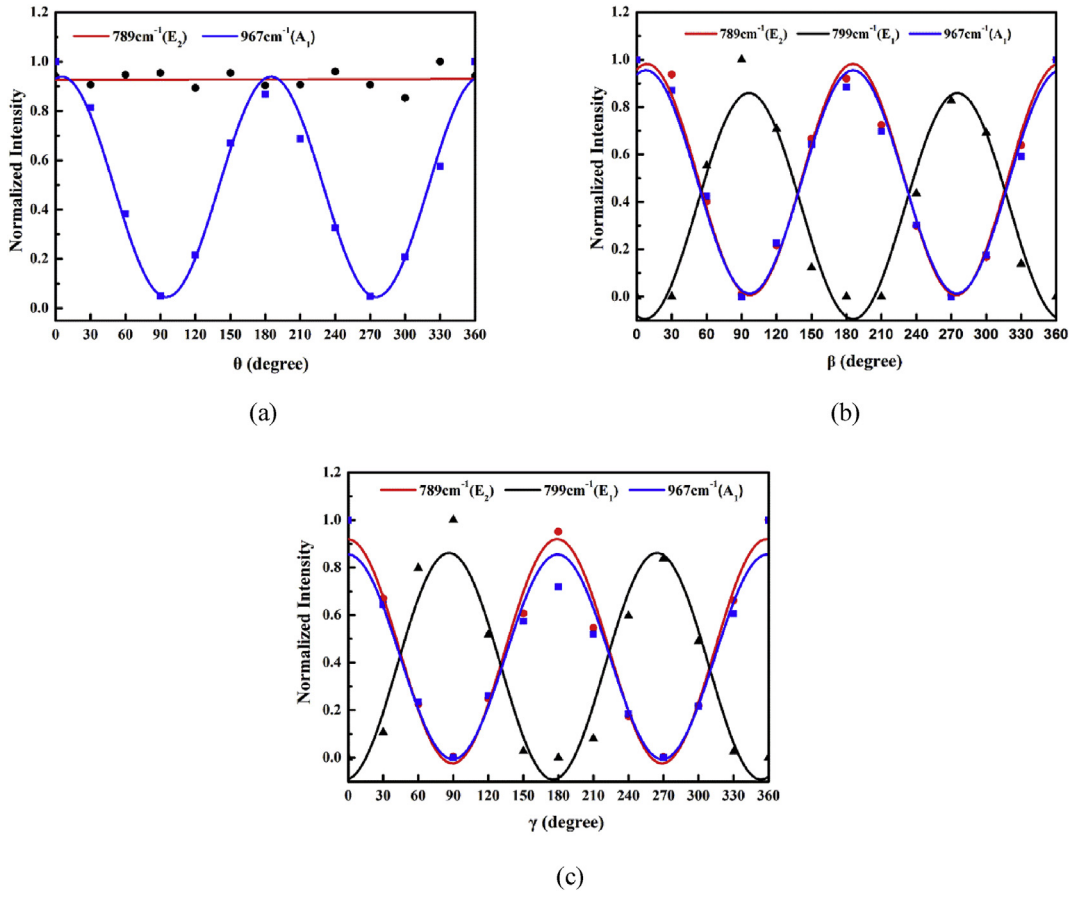


**Fig. 3.** Experimental data and fitting curves for normalized intensity of 6H-SiC collected at different relative angles between the incident and the scattered light, (a) (0001) plane, (b) $(11\bar{2}0)$ plane and (c) $(1\bar{1}00)$ plane.

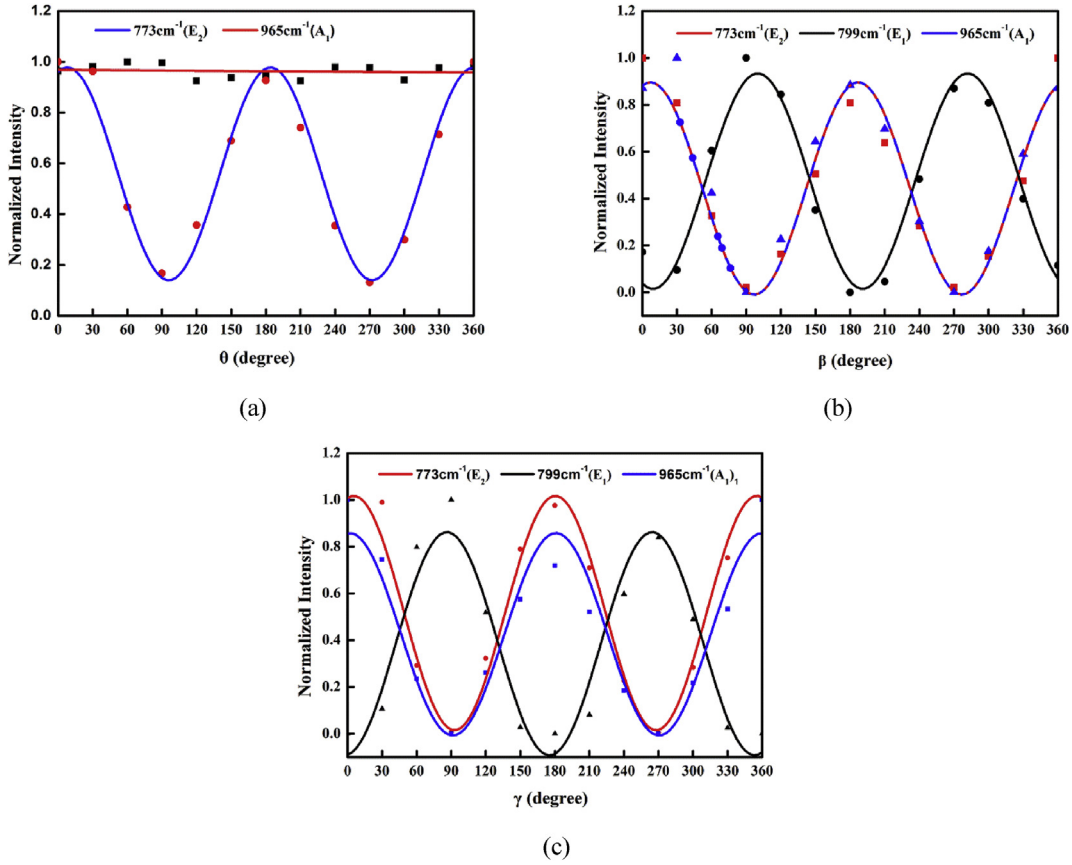


**Fig. 4.** Experimental data and fitting curves for normalized intensity of 4H-SiC collected at different relative angles between the incident and the scattered light, (a) (0001) plane, (b) $(11\bar{2}0)$ plane and (c) $(1\bar{1}00)$ plane.

$$\frac{d\sigma_s}{d\Omega} \propto \left| e_i \bullet \frac{d\alpha}{d\xi} e_s \right|^2 \tag{2}$$

Obviously, the Raman scattering efficiency is determined by the relative directions of the unit vector of $e_i$ and $e_s$. As is described in Fig. 1(b), the unit vector of the direction of incident light and scattered light can be written as:

$$\mathrm{e}_{i(\hat{0\bar{0}01})} = (\cos\theta, \sin\theta, 0),\ \mathrm{e}_{s(\hat{0\bar{0}01})} = (1,0,0),$$

$$\mathrm{e}_{i(\hat{11\bar{2}0})} = (\cos\beta, 0, \sin\beta),\ \mathrm{e}_{s(\hat{11\bar{2}0})} = (1,0,0),$$

$$\mathrm{e}_{i(\hat{1\bar{1}00})} = (0, \cos\gamma, \sin\gamma),\ \mathrm{e}_{s(\hat{1\bar{1}00})} = (0,1,0),$$

The phonon anisotropy properties of 4H and 6H-SiC can be explained by group theory. Wurtzite 4H-SiC and 6H-SiC belong to $C_{6V}$ space group, and the Raman tensors are as follows [26]:

$$\underset{A_1(z)}{\begin{pmatrix} a & 0 & 0 \\ 0 & a & 0 \\ 0 & 0 & b \end{pmatrix}} \quad \underset{E_1(x)}{\begin{pmatrix} 0 & 0 & c \\ 0 & 0 & 0 \\ c & 0 & 0 \end{pmatrix}} \quad \underset{E_1(y)}{\begin{pmatrix} 0 & 0 & 0 \\ 0 & 0 & c \\ 0 & c & 0 \end{pmatrix}} \quad \underset{E_2}{\begin{pmatrix} 0 & d & 0 \\ d & 0 & 0 \\ 0 & 0 & 0 \end{pmatrix}} \quad \underset{E_2}{\begin{pmatrix} d & 0 & 0 \\ 0 & -d & 0 \\ 0 & 0 & 0 \end{pmatrix}}$$

The Raman scattering intensity of $E_1$, $E_2$ and $A_1$ modes in the (0001) plane of wurtzite SiC can be written as:

$$\frac{d\sigma_s}{d\Omega}_{(E_1)} \propto \left| \begin{pmatrix} 1 \\ 0 \\ 0 \end{pmatrix}^T \begin{pmatrix} 0 & 0 & c \\ 0 & 0 & 0 \\ c & 0 & 0 \end{pmatrix} \begin{pmatrix} \cos\theta \\ \sin\theta \\ 0 \end{pmatrix} \right|^2 + \left| \begin{pmatrix} 1 \\ 0 \\ 0 \end{pmatrix}^T \begin{pmatrix} 0 & 0 & 0 \\ 0 & 0 & c \\ 0 & c & 0 \end{pmatrix} \begin{pmatrix} \cos\theta \\ \sin\theta \\ 0 \end{pmatrix} \right|^2 \propto 0 \tag{3}$$

$$\frac{d\sigma_s}{d\Omega}_{(E_2)} \propto \left| \begin{pmatrix} 1 \\ 0 \\ 0 \end{pmatrix}^T \begin{pmatrix} 0 & d & 0 \\ d & 0 & 0 \\ 0 & 0 & 0 \end{pmatrix} \begin{pmatrix} \cos\theta \\ \sin\theta \\ 0 \end{pmatrix} \right|^2 + \left| \begin{pmatrix} 1 \\ 0 \\ 0 \end{pmatrix}^T \begin{pmatrix} d & 0 & 0 \\ 0 & -d & 0 \\ 0 & 0 & 0 \end{pmatrix} \begin{pmatrix} \cos\theta \\ \sin\theta \\ 0 \end{pmatrix} \right|^2 \propto d^2 \tag{4}$$

$$\frac{d\sigma_s}{d\Omega}_{(A_1)} \propto \left| \begin{pmatrix} 1 \\ 0 \\ 0 \end{pmatrix}^T \begin{pmatrix} a & 0 & 0 \\ 0 & a & 0 \\ 0 & 0 & b \end{pmatrix} \begin{pmatrix} \cos\theta \\ \sin\theta \\ 0 \end{pmatrix} \right|^2 \propto a^2(\cos\theta)^2 \tag{5}$$

Available by Eq. (3), the Raman scattering efficiency of the $E_1$ phonon modes in the (0001) plane of 4H and 6H-SiC was supposed to be extinction. Meanwhile, Raman scattering efficiency of $E_2$ modes was calculated to be independent of the relative directions of the incident and the scattered light, whereas, $A_1$ modes exhibited a square cosinusoidal dependence, as plotted in Eqs. (4) and (5).

However, theoretical calculations of $E_1$ modes in the (0001) plane of 4H and 6H-SiC were partially inconsistent with the test results. Coincided with theoretical calculations, $E_1$ mode of 266 $cm^{-1}$ was extinct in the (0001) plane, as showed in Fig. 3(a). Unexpectedly, $E_1$ mode of 799 $cm^{-1}$ in the (0001) plane of appeared and periodicity changed related to the relative directions of the incident and the scattered light, as illustrated in Fig. 5. By contrasting the theoretical and experimental results, the particularity of $E_1$ mode of 799 $cm^{-1}$ was proved. Practically, the appearance of $E_1$ mode of 799 $cm^{-1}$ was caused by the stacking faults in SiC and the intensity relied on the density of stacking fault [27–29]. Analogously to the $(11\bar{2}0)$ and $(1\bar{1}00)$ plane, the normalized intensity of $E_1$ mode of 799 $cm^{-1}$ in the (0001) plane of 4H and 6H SiC showed similar square sinusoidal dependence, as presented in Fig. 5 (c).

Homoplastically, Raman selection rules in different polar planes of hexagonal wurtzite SiC can be obtained by theoretical calculation and experimentation, as showed in Table 2. The Raman selection rules for the phonon modes shown in Table 2 are the curve fitting results of the normalized intensity of each peak. By comparison, it is not difficult to find that the theoretical phonon anisotropy properties of hexagonal wurtzite SiC were consistent with the experimental results, except for the $E_1$ mode of 799 $cm^{-1}$, as showed in Figs. 3 and 4.

### 3.2. Phonon anisotropic properties of 15R-SiC in (0001) plane

Comparable experiment was developed to investigate the phononic anisotropy of 15R-SiC in the (0001) plane, as showed in Fig. 6(a). Similar to the hexagonal wurtzite, the intensity of $A_1$ mode of 965 $cm^{-1}$ in the (0001) plane hinged on the relative directions of the unit vector of $\mathrm{e}_{\hat{i}}$ and $\mathrm{e}_{\hat{s}}$, and revealed a square cosinusoidal dependence on the relative angle. Simultaneously, as showed in Fig. 6(b), the plane mode E in the (0001) plane was expected to be isotropic as displayed in Eq. (7), as the planar acoustic mode E of 172 $cm^{-1}$,786 $cm^{-1}$ and optical mode E of 771 $cm^{-1}$ exhibited isotropic properties. However, similar particularity of E (799 $cm^{-1}$) of 15R-SiC in the (0001) plane discovered. In accordance with 4H and 6H-SiC, the plane optical mode E (799 $cm^{-1}$) emerged owing to stacking fault, and evinced a square cosinusoidal dependence on

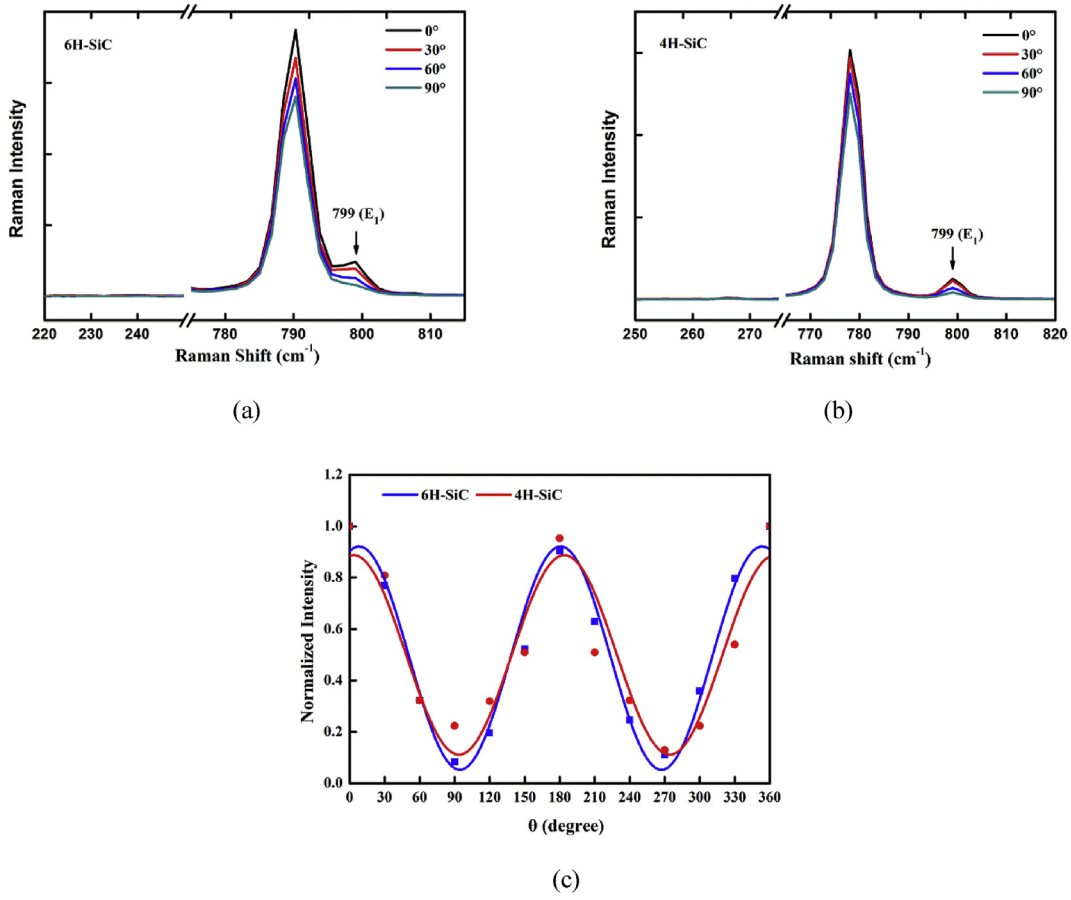


**Fig. 5.** Raman scattering of $E_1$ (799 $cm^{-1}$) mode in the (0001) plane of SiC measured at different relative angles between the incident and the scattered light, (a) 6H-SiC, (b) 4H-SiC, (c) Experimental data and fitting curves for normalized intensity of 4H and 6H-SiC collected at different relative angles between the incident and the scattered light.

**Table 2**
Phonon anisotropic characteristics and Raman selection rules.

| | Polytype | Phonon mode | Peak position ($cm^{-1}$) | (0001)-plane | $(11\bar{2}0)$- plane | $(1\bar{1}00)$- plane |
|---|---|---|---|---|---|---|
| Calculation | 4H/6H | $E_1$ | | $I = 0$ | $I \propto c^2(\sin\beta)^2$ | $I \propto c^2(\sin\gamma)^2$ |
| | | $E_2$ | | $I \propto d^2$ | $I \propto d^2(\cos\beta)^2$ | $I \propto d^2(\cos\gamma)^2$ |
| | | $A_1$ | | $I \propto a^2(\cos\theta)^2$ | $I \propto a^2(\cos\beta)^2$ | $I \propto a^2(\cos\gamma)^2$ |
| | 15R | E | | $\propto d^2$ | $I \propto e^2 + (d^2 - e^2)\cos^2\beta$ | $I \propto (d^2 - e^2 - 2de)\cos^2\gamma + e^2 + de$ |
| | | $A_1$ | | $I \propto a^2\cos^2\theta$ | $I \propto a^2\cos^2\beta$ | $\propto a^2\cos^2\gamma$ |
| Experiment | 4H | $E_1$ | 266 | $I = 0$ | Weak and anisotropic | Weak and anisotropic |
| | | | 799 | $I = 0.11 + 0.78\sin^2[\theta + 41.85]$ | $I = -0.09 + 0.95\sin^2[\beta + 48.08]$ | $I = 0.01 + 0.92\sin^2[\gamma + 35.43]$ |
| | | $E_2$ | 204 | Isotrospoy | Weak and anisotropic | Weak and anisotropic |
| | | | 773 | Isotrospoy | $I = 0.02 + \cos^2[\beta + 38.36)]$ | $I = 0.01 + 0.91\cos^2[\gamma + 37.97]$ |
| | | $A_1$ | 612 | Weak and anisotropic | Weak and anisotropic | Weak and anisotropic |
| | | | 965 | $I = 0.01 + 0.84\cos^2[\theta + 36.93]$ | $I = 0.01 + 0.87\cos^2[\beta + 43.05]$ | $I = 0.02 + 0.90\cos^2[\gamma + 31.07]$ |
| | 6H | $E_1$ | 240 | $I = 0$ | Weak and anisotropic | Weak and anisotropic |
| | | | 799 | $I = 0.06 + 0.86\cos^2[\theta + 35.00]$ | Weak and anisotropic | $I = -0.09 + 0.95\cos^2[\gamma - 51.67]$ |
| | | $E_2$ | 150 | Isotrospoy | $I = 0.14 + 0.86\cos^2[\beta + 39.82]$ | $I = 0.02 + 0.98\cos^2[\gamma + 44.06]$ |
| | | | 769 | Isotrospoy | $I = 0.08 + 0.77\cos^2[\beta + 41.57]$ | $I = 0.05 + 0.91\cos^2[\gamma + 44.05]$ |
| | | | 789 | Isotrospoy | $I = -0.02 + 0.92\cos^2[\beta + 40.53]$ | $I = 0.01 + 0.98\cos^2[\gamma + 35.51]$ |
| | | $A_1$ | 967 | $I = 0.04 + 0.90\cos^2[\theta + 39.78]$ | $I = 0.01 + 0.79\cos^2[\beta + 41.32]$ | $I = 0.01 + 0.94\cos^2[\gamma + 36.58]$ |
| | 15R | E | 172 | Isotrospoy | – | – |
| | | | 771 | Isotrospoy | – | – |
| | | | 786 | Isotrospoy | – | – |
| | | | 799 | $I = 0.40 + 0.48\cos^2[\theta + 45.04]$ | – | – |
| | | $A_1$ | 965 | $I = 0.35 + 0.52\cos^2[\theta + 47.61]$ | – | – |

*I: Normalized Raman Intensity.

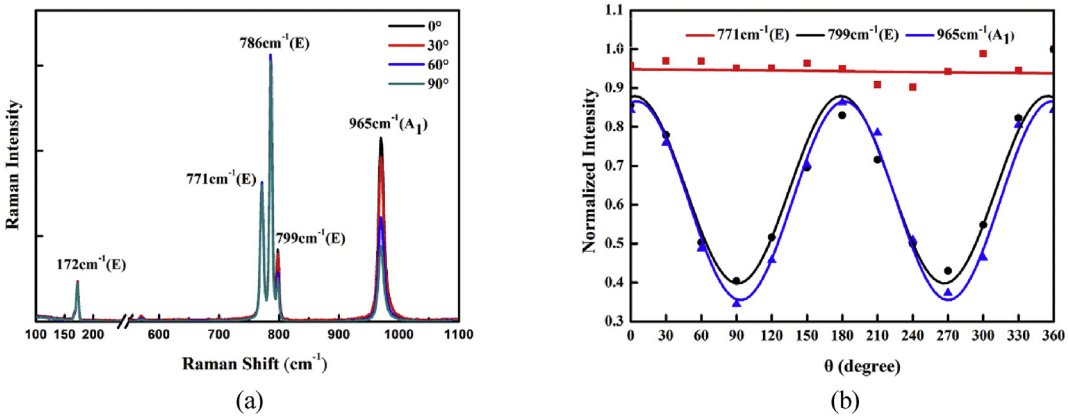


**Fig. 6.** (a) Polarization Raman spectra of 15R-SiC in the (0001) plane collected at different relative angles between the incident and the scattered light. (b) Experimental data and fitting curves for normalized intensity of 15R-SiC with different relative angles between the unit vector of the polarization incident light ($e_i$) and the scattered light ($e_s$).

the relative directions between the incident and the scattered light.

In the (0001) plane of 15R-SiC region, the unit vector of the direction of incident light and scattered light can be written as:

$$e_{\hat{i}} = (\cos\delta, \sin\delta, 0), \quad e_{\hat{s}} = (1, 0, 0)$$

15R-SiC belongs to $C_{3V}^5$ space group, and its Raman tensors are shown as following:

$$\underset{A_{1g}}{\begin{pmatrix} a & 0 & 0 \\ 0 & a & 0 \\ 0 & 0 & b \end{pmatrix}} \quad \underset{A_{2g}}{\begin{pmatrix} 0 & c & 0 \\ -c & 0 & 0 \\ 0 & 0 & 0 \end{pmatrix}} \quad \underset{E_g}{\begin{pmatrix} 0 & d & 0 \\ d & 0 & e \\ 0 & f & 0 \end{pmatrix} \begin{pmatrix} d & 0 & -e \\ 0 & -d & 0 \\ -f & 0 & 0 \end{pmatrix}}$$

The Raman scattering intensity of $E_1$, $E_2$ and $A_1$ modes in the (0001) plane of 15R-SiC can be written as:

$$\frac{d\sigma_s}{d\Omega_{(A_1)}} \propto \left| \begin{pmatrix} 1 \\ 0 \\ 0 \end{pmatrix}^T \begin{pmatrix} a & 0 & 0 \\ 0 & a & 0 \\ 0 & 0 & b \end{pmatrix} \begin{pmatrix} \cos\delta \\ \sin\delta \\ 0 \end{pmatrix} \right|^2 \propto a^2(\cos\delta)^2 \tag{6}$$

Similarly, the calculation results of the phonons anisotropy in 15R-SiC in the $(11\bar{2}0)$ and $(1\bar{1}00)$ planes were provided in Table 2. And surprisingly, the anisotropy of the $A_1$ mode in the $(11\bar{2}0)$ and $(1\bar{1}00)$ plane still showed homogeneous square cosinusoidal dependence on the relative directions. On the contrary, the anisotropy of the planar mode E is not only related to the relative directions of the incident light and the scattered light, but also relevant to the Raman tensors elements which worth further exploration.

## 4. Conclusion

In conclusion, Raman spectra of 4H, 6H and 15R- SiC have been recorded from the (0001), $(11\bar{2}0)$ and $(1\bar{1}00)$ planes of wurtzite SiC as a function of the relative angles between the incident and the scattered. Consistent with the calculation results, $E_2$ and $A_1$ modes in the $(11\bar{2}0)$ and $(1\bar{1}00)$ planes of Wurtzite SiC showed homogeneous anisotropy properties, and the normalized Raman intensity hinged on the relative angles. The isotropy properties of $E_2$ modes in the (0001) plane of wurtzite SiC are available from the group theoretical analysis and Raman test. Specifically, $E_1$ modes in the $(11\bar{2}0)$ and $(1\bar{1}00)$ planes of wurtzite SiC are quite different from those of $A_1$ and $E_2$ modes, and showed a square sinusoidal dependence on the relative angles. According to the group theoretical analysis, $E_1$ modes in the (0001) plane of wurtzite SiC and 15R-SiC were supposed to be prohibited and isotropic, respectively. However, it is unexpected to find the anisotropy properties of the peak 799 $cm^{-1}$ ($E_1$) due to the existence of stacking faults. Otherwise, Raman intensity of E modes in the (0001) plane other than E (799 $cm^{-1}$) of 15R-SiC region exhibits isotropic properties while $A_1$ modes display a square cosinusoidal dependence on the relative directions. For the 15R-SiC in the $(11\bar{2}0)$ and $(1\bar{1}00)$ planes, $A_1$ mode almost invariably exhibited similar anisotropy properties, and the Raman scattering efficiency of the E mode was related to the two factors of the tensor elements and the relative directions.

$$\frac{d\sigma_s}{d\Omega_{(E)}} \propto \left| \begin{pmatrix} 1 \\ 0 \\ 0 \end{pmatrix}^T \begin{pmatrix} 0 & d & 0 \\ d & 0 & e \\ c & f & 0 \end{pmatrix} \begin{pmatrix} \cos\delta \\ \sin\delta \\ 0 \end{pmatrix} \right|^2 + \left| \begin{pmatrix} 1 \\ 0 \\ 0 \end{pmatrix}^T \begin{pmatrix} d & 0 & -e \\ 0 & -d & 0 \\ -f & 0 & 0 \end{pmatrix} \begin{pmatrix} \cos\delta \\ \sin\delta \\ 0 \end{pmatrix} \right|^2 \propto d^2 \tag{7}$$

## Acknowledgements

This work was supported by National R&D Program of China (Grant No. 2016YFB0400501); National Natural Science Foundation of China (Grant No. 51502156,61504075); Joint Foundation of Equipment Development and State Education Ministry for Outstanding Researcher (Grant No. 6141A0232); Science and Technology Project of

State Grid Corporation of China (Grant No. SGSDDK00KJJS1600063, SGSDDK00KJJS1600071); Province Key R&D Program of Shandong (Grant No. 2017CXGC0412,2016GGX4101, 2016ZDJS09A05, 2016ZDJS01B03); Fundamental Research Funds for Natural Science of Shandong University (Grant No.2016JC037).

## Appendix A. Supplementary data

Supplementary data to this article can be found online at https://doi.org/10.1016/j.jallcom.2018.10.324.

## References

[1] R. Madar, Materials science: silicon carbide in contention, Nature 430 (2004) 974–975.
[2] J.B. Casady, R.W. Johnson, Status of silicon carbide (SiC) as a wide-bandgap semiconductor for high-temperature applications: a review, Solid State Electron. 39 (1996) 1409–1422.
[3] A. Itoh, H. Matsunami, Single crystal growth of SiC and electronic devices, C R C Crit. Rev. Solid State Sci. 22 (1997) 111–197.
[4] R. Kirschman, Status of silicon carbide (SiC) as a Wide Bandgap semiconductor for High Temperature applications: a review, Solid State Electron. 39 (2009) 1409–1422.
[5] J. Chen, M. Liu, T. Yang, F. Zhai, X. Hou, K.C. Chou, Improved microwave absorption performance of modified SiC in the 2–18 GHz frequency range, CrystEngComm 19 (2016).
[6] P.R. VANLOAN, A study of polytypism in silicon carbide, Am. Mineral. 52 (1967) 946 (&).
[7] L. Bergman, D. Alexson, C. Balkas, H. Shin, R.F. Davis, Raman analysis of phonon lifetimes in AlN and GaN of wurtzite structure, Phys. Rev. B 59 (1999) 12977–12982.
[8] H.C. Lin, Z.C. Feng, M.S. Chen, Z.X. Shen, I.T. Ferguson, W. Lu, Raman scattering study on anisotropic property of wurtzite GaN, J. Appl. Phys. 105 (2009) 37.
[9] H.C. Lin, Z.C. Feng, M.S. Chen, Z.X. Shen, W.J. Lu, W.E. Collins, Anisotropic properties of GaN studied by Raman scattering, in: Materials Science Forum, 2006.
[10] T. Azuhata, T. Sota, K. Suzuki, S. Nakamura, Polarized Raman spectra in GaN, J. Phys. Condens. Matter 7 (1995) L129.
[11] C. Bundesmann, N. Ashkenov, M. Schubert, D. Spemann, T. Butz, E.M. Kaidashev, M. Lorenz, M. Grundmann, Raman scattering in ZnO thin films doped with Fe, Sb, Al, Ga, and Li, Appl. Phys. Lett. 83 (2003) 1974–1976.
[12] S. Nakashima, T. Mitani, J. Senzaki, H. Okumura, T. Yamamoto, Deep ultraviolet Raman scattering characterization of ion-implanted SiC crystals, J. Appl. Phys. 97 (2005), 123507-123507-8.
[13] J.C. Burton, F.H. Long, I.T. Ferguson, Resonance enhancement of electronic Raman scattering from nitrogen defect levels in silicon carbide, J. Appl. Phys. 86 (1999) 2073–2077.
[14] F.J. Campos, N. Mestres, J. Pascual, E. Morvan, P. Godignon, J. Millan, Confocal micro-Raman characterization of lattice damage in high energy aluminum implanted 6H-SiC, J. Appl. Phys. 85 (1999) 99–104.
[15] S. Nakashima, H. Harima, Raman investigation of SiC polytypes, Phys. Status Solidi 162 (1997) 39–64.
[16] H. Harima, S.I. Nakashima, T. Uemura, Raman scattering from anisotropic LO-phonon–plasmon-coupled mode in n-type 4H-and 6H-SiC, J. Appl. Phys. 78 (1995) 1996–2005.
[17] M.V. Klein, B.N. Ganguly, P.J. Colwell, Theoretical and experimental study of Raman scattering from coupled LO-phonon-plasmon modes in silicon carbide, Phys. Rev. B 6 (1972) 2380.
[18] H. Yugami, S. Nakashima, A. Mitsuishi, A. Uemoto, Characterization of the free-Carrier concentrations in doped β-SiC crystals by Raman scattering, J. Appl. Phys. 61 (1987) 354–358.
[19] W. Liu, T. Yang, J. Chen, Y. Chen, X. Hou, X. Han, K.C. Chou, Improvement in surface-enhanced Raman spectroscopy from cubic SiC semiconductor nanowhiskers by adjustment of energy levels, Phys. Chem. Chem. Phys. 18 (2016) 27572–27576.
[20] D. Nakamura, I. Gunjishima, S. Yamaguchi, T. Ito, A. Okamoto, H. Kondo, S. Onda, K. Takatori, Ultrahigh-quality silicon carbide single crystals, Nature 430 (2004) 1009–1012.
[21] D.W. Feldman, J.H.P. Jr, W.J. Choyke, L. Patrick, Phonon dispersion curves by Raman scattering in SiC, polytypes 3C, 4H, 6H, 15R, and 21R, Phys. Rev. 173 (1968) 787–793.
[22] D.W. Feldman, J.H. Parker, W.J. Choyke, L. Patrick, Raman scattering in 6H SiC, Phys. Rev. 170 (1968) 698–704.
[23] J.C. Burton, Characterization of silicon carbide using Raman spectroscopy/, in: Materials Science Forum, 2000.
[24] L. Patrick, Infrared absorption in SiC polytypes, Phys. Rev. 167 (1968) 809–813.
[25] M. Cardona, R.K. Chang, G. Güntherodt, M.B. Long, H. Vogt, Light Scattering in Solids II, Basic Concepts and Instrumentation, 1982.
[26] R. Loudon, The Raman effect in crystals, Adv. Phys. 13 (1964) 813–864.
[27] S. Nakashima, Y. Nakatake, H. Harima, M. Katsuno, Detection of stacking faults in 6H-SiC by Raman scattering, Appl. Phys. Lett. 77 (2000) 3612–3614.
[28] R. Stevens, Defects in silicon carbide, J. Am. Ceram. Soc. 7 (1972) 517–521.
[29] H.P. Iwata, U. Lindefelt, S. Öberg, P.R. Briddon, Stacking faults in silicon carbide, Phys. B Condens. Matter 340 (2003) 165–170.